

水旋風分離器溢流管結構對分級效率的影響

陳建宏 吳容銘*

淡江大學化學工程與材料工程學系

摘要

本研究使用三相流方法模擬四種不同溢流管結構之水旋風分離器之分級效率，此四種不同溢流管結構分別為內徑 9 mm 之直管、入口 12 mm 出口 9 mm 之擴散管、入口 9 mm 出口 12 mm 之收縮管、以及 12 mm 之直管，研究結果顯示在相同之操作條件下，具收縮狀之溢流管可獲得較澄清且較大量之溢流。

關鍵詞：計算流體力學，模擬，水旋風分離器，顆粒大小，模型。

THE EFFECTS OF A HYDROCYCLONE OVERFLOW PIPE STRUCTURE ON SEPARATION EFFICIENCY

Chien-Hung Chen Rome-Ming Wu*

Department of Chemical and Materials Engineering
Tamkang University
Danshui, Taiwan 251, R.O.C

Key Words: computational fluid dynamics, simulation, hydrocyclones, particle size, modelling.

ABSTRACT

This study applied three-phase flow simulation to simulate the effect of four different types of overflow pipes on clarification. These four types of overflow pipes include: a 9 mm straight pipe (9-9), divergent overflow pipe (9-12), convergent overflow pipe (12-9), and a 12 mm straight pipe (12-12). The results indicate that under similar split ratios and other variables of similar operations, the converge type overflow pipe can obtain much more supernatant liquid, with greatly improved separation efficiency.

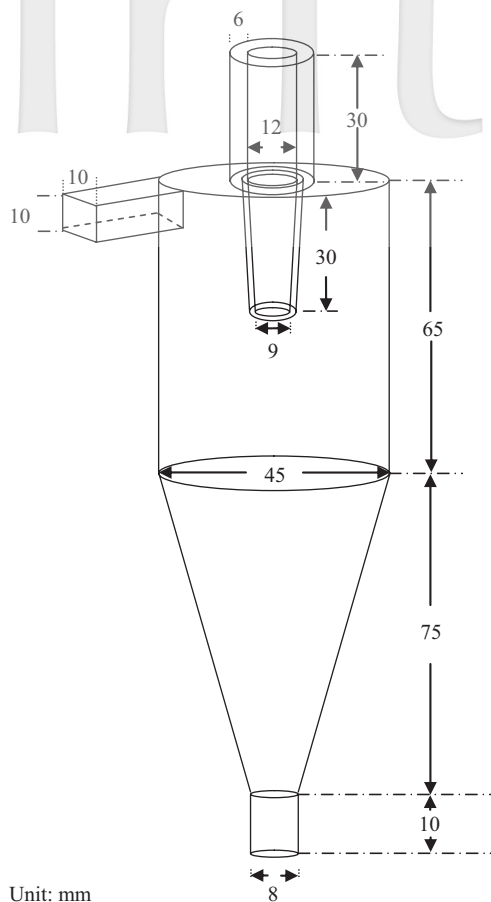
I. INTRODUCTION

Hydrocyclone is favored classifying equipment for solids separation [1, 2]. Its applications are in mineral processing [3], and to a growing extent, in dewatering [4], deoiling [5], and water treatment [6], etc.

In the past, many efforts have been made to develop efficient hydrocyclones by designing the hydrocyclones with some new structures to change the flow characteristics of conventional hydrocyclones. For example, the water injected hydrocyclone [7] was developed to interrupt the boundary layer flow to diminish the fine particle

*通訊作者：吳容銘，e-mail: romeman@mail.tku.edu.tw

Corresponding author: Rome-Ming Wu, e-mail: romeman@mail.tku.edu.tw



Unit: mm

Fig. 1 Geometry of the hydrocyclone separator used for both CFD simulations and experiments.

content in the underflow. Changirwa *et al.* [8] proposed a hybrid hydrocyclone with one feed entry and three exits that can separate oil, water, and sand, respectively. Lee and Williams [9] recommended inserting a long rod into the hydrocyclone. It may also be seen that the recovery of smaller particle sizes was enhanced in the presence of the rod. This might have some benefit if the hydrocyclone is to be used for classification. Asomah and Napier-Munn [10] indicate that cyclone inclination significantly affects hydrocyclone performance; particularly for larger, low pressure cyclones at inclinations of 45° or greater. Grommers *et al.* [11] highlight that, after testing a total of 26 different hydrocyclones, the hydrocyclone geometry design factors that are particularly important are the underflow diameter and the depth of the vortex finder.

In terms of other aspects that are relevant to the overflow pipe design, Shah *et al.* [12] show that, from the coefficients of the individual models developed, it is evident that the vortex finder diameter has a more pronounced effect on water split (or split ratio, defined as volumetric

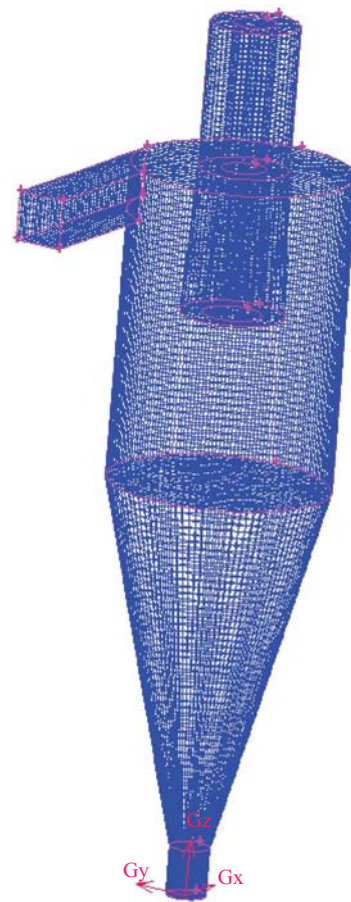


Fig. 2 Mesh structure of the hydrocyclone separator. The total number of computational cells is 101,280.

flow rate of underflow/overflow) than the spigot diameter and feed pressure. Mainza *et al.* [13] proposed a hydrocyclone with one underflow opening and two overflow openings. The main function of the dual vortex finders in a three-product cyclone is to prevent the short-circuiting of coarse material into the overflow, and to promote preferential separation of the material reporting to the inner and outer overflow streams.

With developments in science and technology, mathematical models based on computational fluid dynamics (CFD) are highly desirable for solving flow fields in a hydrocyclone [14, 15], clarifier [16], etc. However, the complexity of the flow pattern of a hydrocyclone separator, changes in the air core pattern, and the CFD of unsteady flow were seldom discussed.

The objective of this study is to investigate the flow pattern and particle tracing of a hydrocyclone with different overflow pipe shape through FLUENT. Three-dimensional, VOF multiphase flow model, and the LES turbulence model were used to explore the effect of overflow

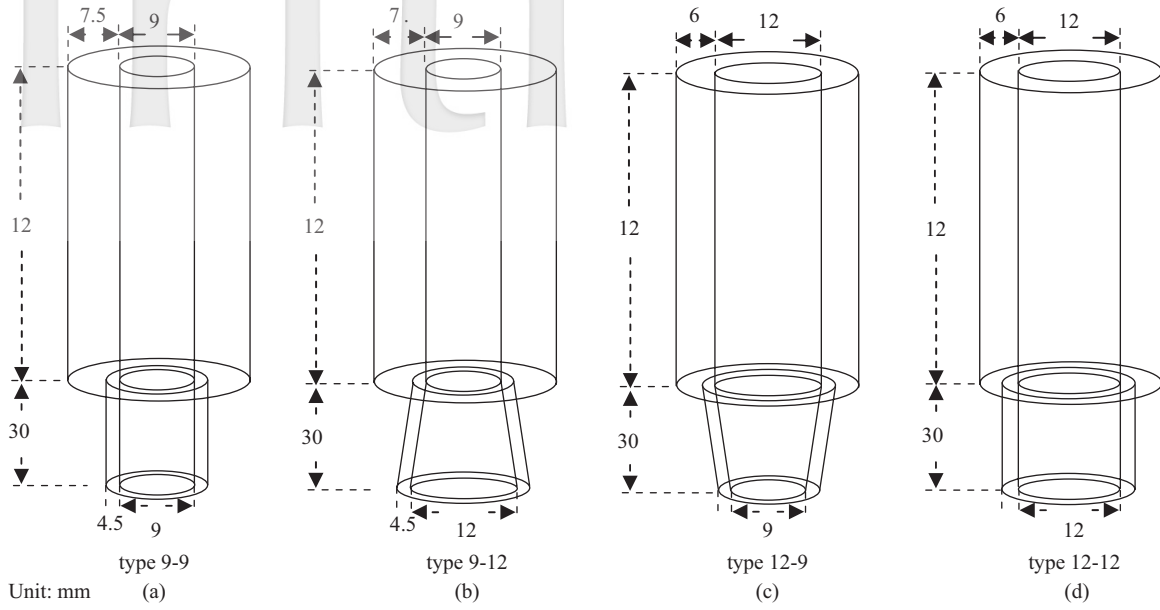


Fig. 3 Geometries and sizes of the four types of overflow pipes.

pipe shape on separation efficiency.

II. NUMERICAL METHODS

1. Geometry and Meshes

The geometry and meshes of this hydrocyclone are displayed in Fig. 1 and Fig. 2. The diameters of underflow and hydrocyclone were 8 and 45 mm, respectively. The length of the cylindrical part was 65 mm, while the length of the cone part was 75 mm, making an overall cone angle. The hybrid mesh volumes used in this study is 101,280. The overflow pipe section consisted of pipes with two ends of different diameters; one of 12 mm and another of 9 mm. Changes in the combination of exit and entrance for the overflow separately created four different types of overflow pipes. They include 9 mm straight pipes (9-9), divergent overflow pipes (9-12), convergent overflow pipes (12-9), and 12 mm straight pipes (12-12) (Fig. 3).

2. Turbulence Model

Only the DSM and LES provide implicit accounting for local turbulence asymmetry, and therefore it is only models like these that are able to accurately capture the detail of the hydrocyclone flow field, as demonstrated by Slack *et al.* [17]. Thus, we applied the LES turbulent model in our simulation. LES is a transient simulation that requires grid that is 3D and finer than other grids.

Therefore, grid independence studies were conducted, and it was determined that once the number of elements were halved and doubled, the solutions of the velocity field showed a maximum difference of 5.1% between the consecutive grids.

A filtered variable (denoted by an overbar) is defined by:

$$\bar{\phi}(X) = \int_D \phi(X') G(X, X') dX' \quad (1)$$

where D is the fluid domain, and G is the filter function that determines the scale of the resolved eddies. In the commercial CFD code FLUENT, the filtering operation is implicitly embedded within the finite-volume discretization process:

$$\bar{\phi}(X) = \frac{1}{V} \int_V \phi(X') dX', X' \in V \quad (2)$$

where V is the volume of a computational cell. The filter function, $G(X, X')$, implied here is then:

$$G(X, X') = \begin{cases} 1/V, & X' \in V \\ 0, & X' \text{ otherwise} \end{cases} \quad (3)$$

Filtering the Navier-Stokes equations, one obtains:

$$\frac{\partial \rho}{\partial t} + \frac{\partial}{\partial x_i} (\rho \bar{u}_i) = 0 \quad (4)$$

$$\frac{\partial}{\partial t}(\rho \bar{u}_i) + \frac{\partial}{\partial x_j}(\rho \bar{u}_i \bar{u}_j) = \frac{\partial}{\partial x_j} \left(\mu \frac{\partial \sigma_{ij}}{\partial x_j} \right) - \frac{\partial \bar{p}}{\partial x_j} - \frac{\partial \tau_{ij}}{\partial x_j} \quad (5)$$

where σ_{ij} is the stress tensor due to molecular viscosity defined by:

$$\sigma_{ij} = \left[\mu \left(\frac{\partial \bar{u}_i}{\partial x_j} + \frac{\partial \bar{u}_j}{\partial x_i} \right) \right] - \frac{2}{3} \mu \frac{\partial \bar{u}_l}{\partial x_l} \delta_{ij} \quad (6)$$

and τ_{ij} is the subgrid-scale stress defined by:

$$\tau_{ij} \equiv \overline{\rho u_i u_j} - \rho \bar{u}_i \bar{u}_j \quad (7)$$

3. Initial and Boundary Conditions

The inlet fluid is moving at a constant speed, and the boundary condition is as follows:

$$\vec{v} = \text{constant} \quad @ \text{ inlet pipe} \quad (8)$$

The outlet fluid is moving under the absolute pressure of 1 atm; therefore, the gauge pressure at underflow/overflow is zero. The boundary conditions are:

$$P = 0 \quad @ \text{ underflow} \quad (9)$$

$$P = 0 \quad @ \text{ overflow} \quad (10)$$

No-slip boundary conditions were applied on all walls of the hydrocyclone. The computational fluid dynamics program, FLUENT 6.1 (Fluent Inc., USA), solved the governing equations (Eqns. 4-7), together with the associated initial and boundary condition equations (Eqns. 8-10). The pressure staggered option (PRESTO) was adopted, which is a pressure interpolation scheme reported as useful for predicting the high swirl flow characteristics that prevail inside the hydrocyclone body. The SIMPLE algorithm scheme was applied, which uses a combination of continuity and momentum equations to derive an equation for pressure. Interpolation for field variables, from cell centers to the faces of the control volumes with a higher-order quadratic upwind interpolation (QUICK) spatial discretization scheme was used. The calculations were carried out with the maximum relative error of 10⁻⁴ for fluid velocity evaluations.

III. EXPERIMENTAL METHOD

Silicon oxide powder with a density of 2200 kg/m³

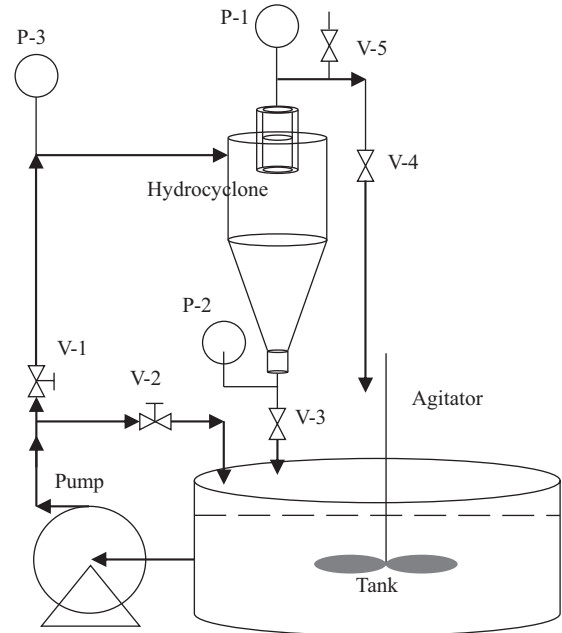


Fig. 4 Experimental setup of the hydrocyclone separator system. The various components include a centrifugal pump, storage tank, agitator, pressure gauges (P-1, P-2, P-3), recycle valve (V-2), inlet valve (V-1), overflow valve (V-4), underflow valve (V-3), relief valve (V-5) and the hydrocyclone separator.

was used in the experiments carried out in this study. A laser light scattering facility (Horiba LA-950, 0.01-3000 μm) with a 650 nm He-Ne laser and a 405 nm LED light as the light source was used for size characterization of the powder, and the average particle diameter was about 16.5 μm .

A suspension of desired mass concentration was prepared prior to each experiment. The storage tank was filled with 60 L of water, and a known mass of powder was added to form a 0.3 wt% suspension. Fig. 4 shows the configuration of the overall experimental setup used, which includes various components such as a centrifugal pump, storage tank, agitator, pressure gauges, valves, and the hydrocyclone separator.

IV. RESULTS AND DISCUSSION

1. Separation efficiency curve and concentration

Fig. 5 shows the separation efficiency curve under various pressures at a split ratio of 1.0. As shown in the diagram, when the size of the overflow pipe entrance is smaller (as with the type 12-9 and 9-9, solid symbols), it

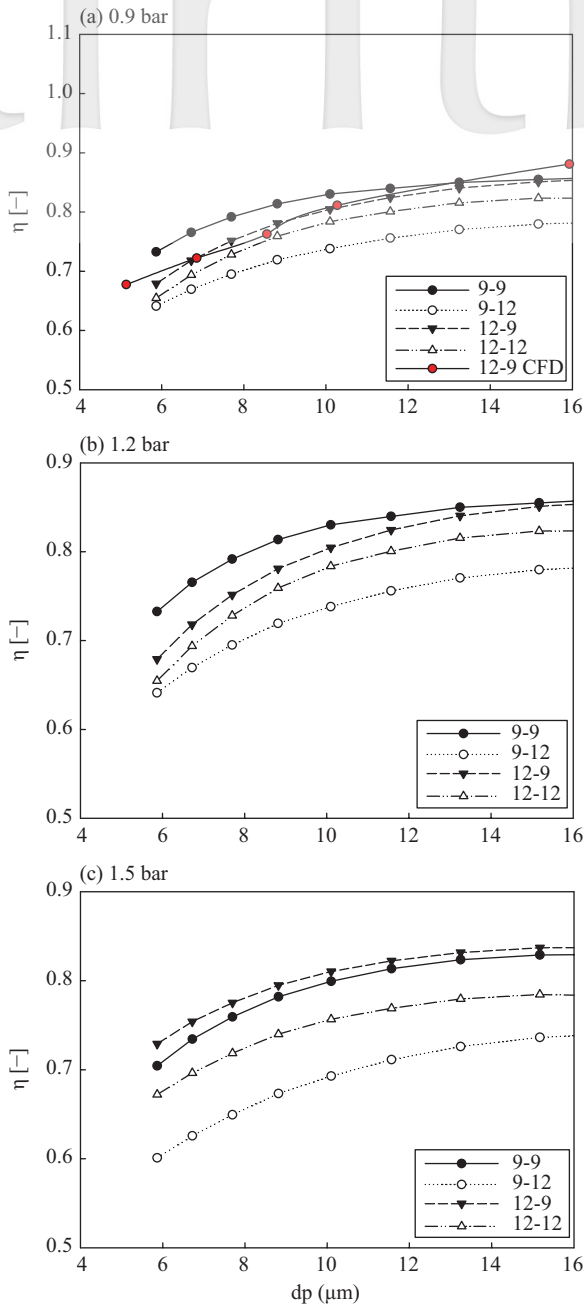


Fig. 5 Experimental separation efficiency curves of the four hydrocyclone separators (a) 0.9 bar (b) 1.2 bar (c) 1.5 bar. (Only the red symbol solid line is from CFD)

does not facilitate particle flow through the overflow, so it must flow out through the underflow instead. Therefore, its curve efficiency is higher; when comparing 12-9 to 12-12 (Fig. 5(c)), the underflow flow rate of particles through 12-9 increased by about 0.05. In other words, under the same flow split ratio, type 12-9 and 9-9 overflow pipes can obtain better supernatant liquids and more

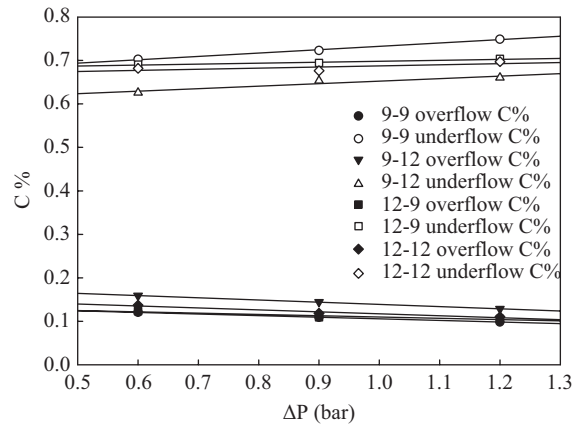


Fig. 6 Solid concentrations of underflow and overflow under different operational pressures.

concentrated fluids. This is also described in a diagram in Fig. 6 showing the overflow and underflow concentration as a result of changing operating pressures. As seen, when the operating pressure is greater, the overflow concentration is lower and the underflow concentration is higher. Among various overflow pipes, type 12-9 and 9-9 overflow pipes can obtain better supernatant liquids and more concentrated fluids. Simulation and experimental results from type 12-9 overflow pipes, as represented by the red solid circle in Fig. 5(a), are consistent.

Fig. 7 shows an efficiency increase of about 0.05 under a fixed operating pressure during a higher flow split rate, i.e., when the underflow is large. The integration of the results from these two diagrams indicates that if a large quantity of supernatant liquid is to be obtained, the first task is to appropriately increase the flow split ratio and then replace the overflow pipes with pipes of the convergent type. Hashmi *et al.* [18] proposed an adjustable overflow orifice. The overflow orifice's size in the CANMET hydrocyclone can be changed during operation to provide an additional measure of performance control. Therefore, in practice, a hydrocyclone with an adjustable overflow pipe diameter can be designed to achieve separation.

2. Particle Tracks

To further understand the trajectory of particles when the overflow pipe changes shape, ten location points in the hydrocyclone were selected for particle release so that their trajectories could be observed, as shown in Fig. 8. Using position 8 to serve as an example, Fig. 9 shows a trajectory diagram for different sized particles. In type 9-9 and 12-9 overflow pipes, large particles are still affected by centrifugal force, forcing them to move towards

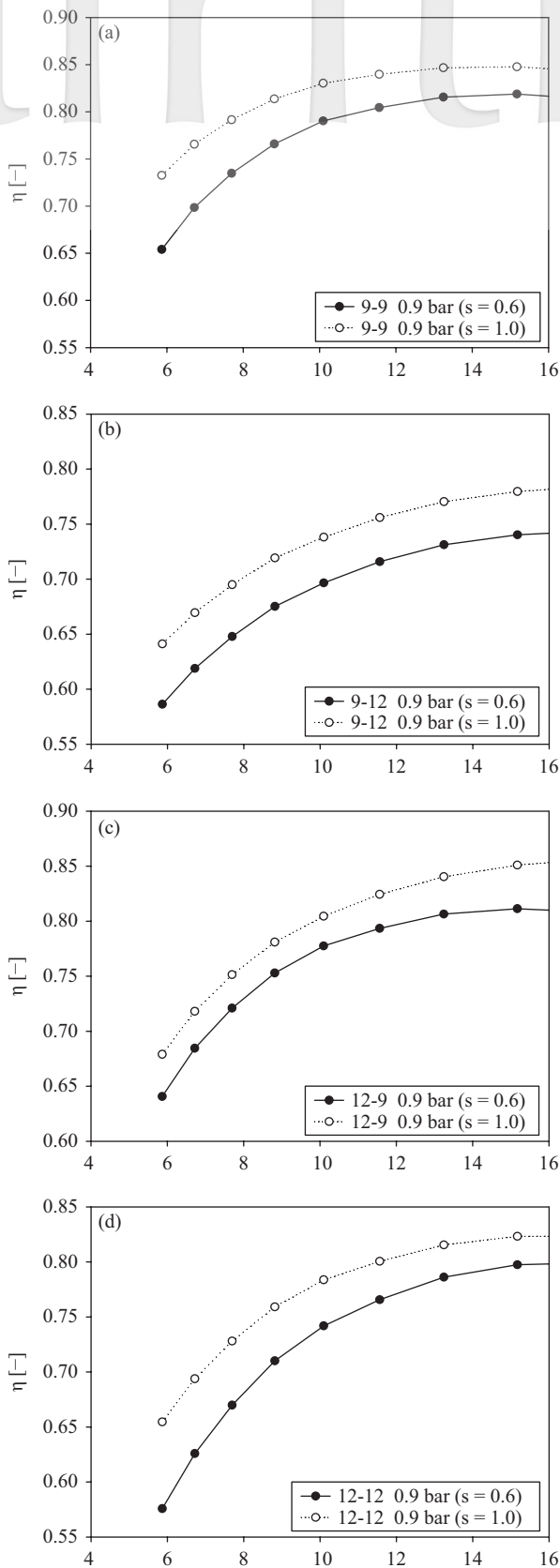


Fig. 7 Experimental separation efficiency of the four hydrocyclone separators (a) 9-9 type (b) 9-12 type (c) 12-9 type (d) 12-12 type.

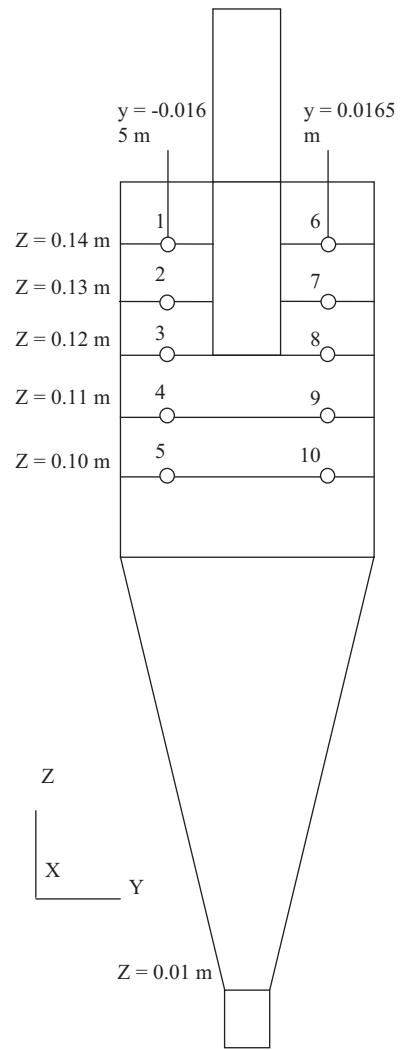


Fig. 8 Particles release positions used in CFD.

the underflow. However, for type 9-12 and 12-12 overflow pipes, large particles are observed flowing out of the overflow through the short circuit, resulting in poor separation.

Reasons for this phenomenon can be determined by Fig. 10, which shows the axial velocity distribution diagram with a color map ranging from -7 m/s to 7 m/s, where red represents upward moving velocity, and blue represents the downward velocity. As shown in Fig. 10 (d), the periphery of the middle air core includes an upward speed zone, which can easily carry particles towards the overflow. The entrance to the overflow pipe also includes a large upward speed zone. With a larger area, short-circuit flow can be created more easily. As shown in Fig. 10(a) and 10(c), since the periphery of the middle air core area covered by the upward speed zone is smaller than Fig. 10(d), and the entrance of the overflow pipe has

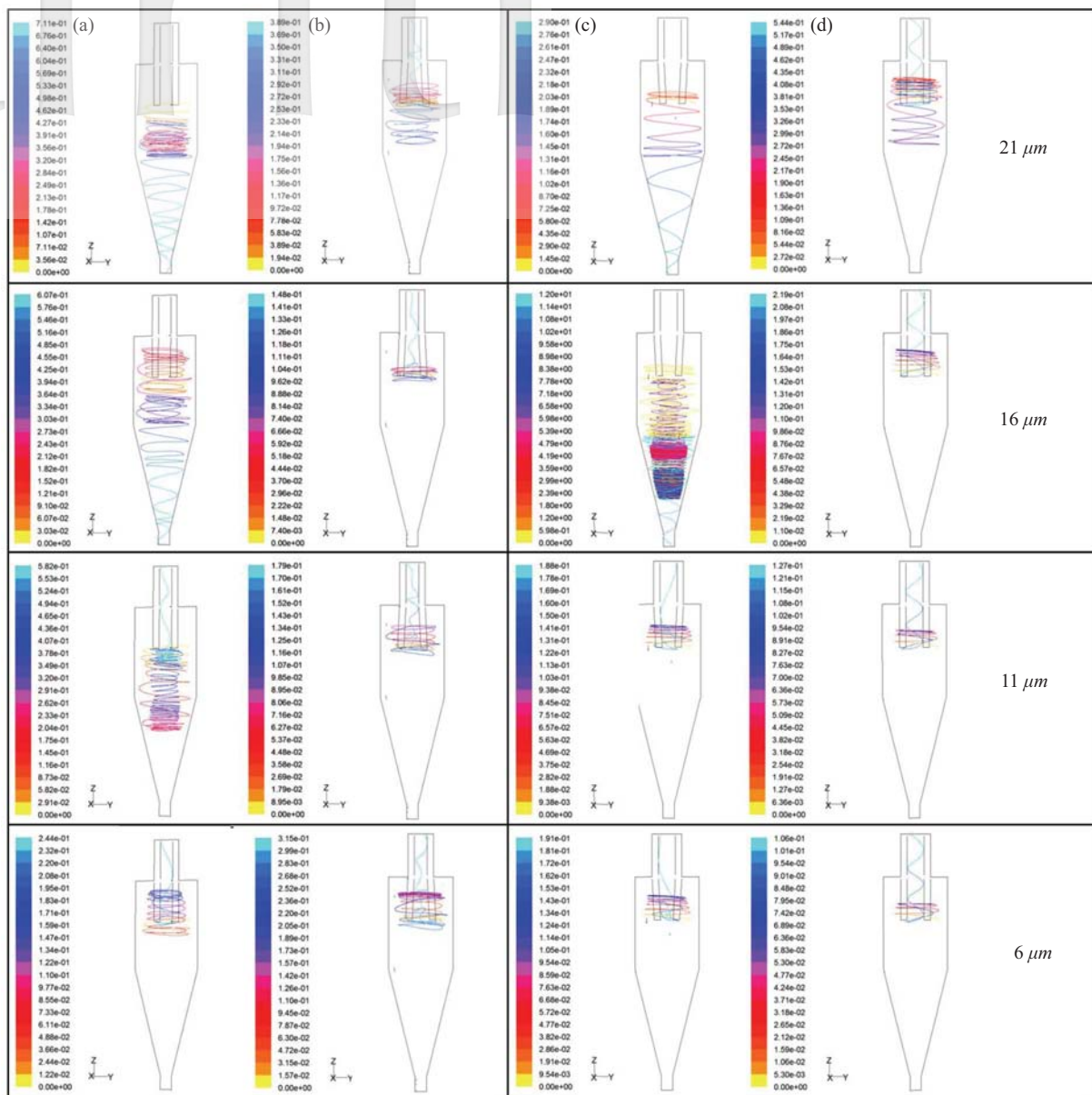


Fig. 9 Different size particles released at position No. 8 finally reported to overflow/underflow (a) type 9-9 (b) type 9-12 (c) type 12-9 (d) type 12-12.

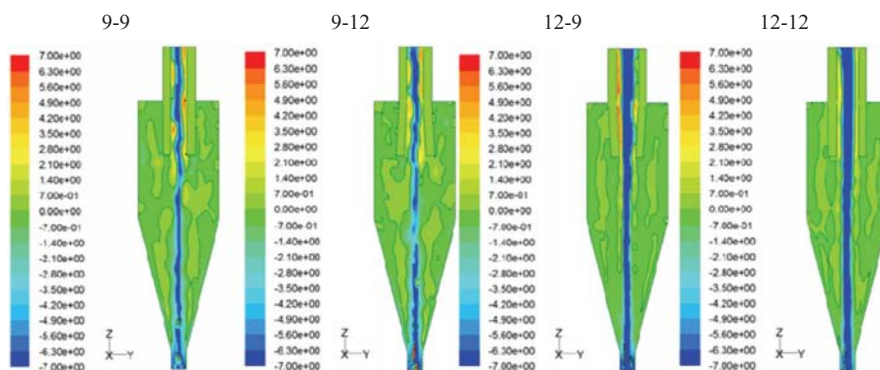


Fig. 10 Velocity contour of vertical velocity in the four different hydrocyclones (a) type 9-9 (b) type 9-12 (c) type 12-9 (d) type 12-12.

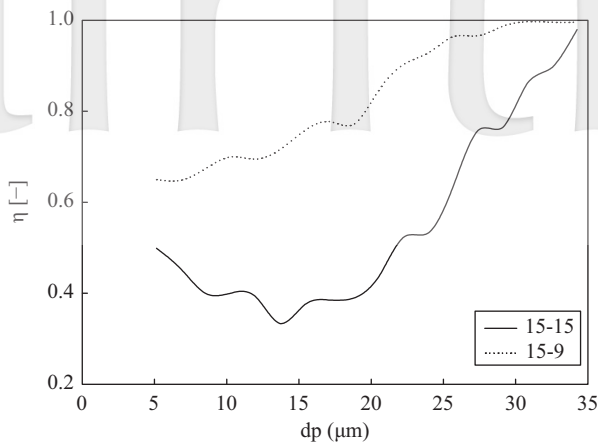


Fig. 11 Simulation efficiency curve of 15-15 type and 15-9 type hydrocyclone.

no upward speed zone, a short-circuit flow cannot be easily created. As shown in Fig. 10(b), although the upward speed zone covering the periphery of the middle air core has disappeared, there is a larger forward speed zone at the entrance of the overflow pipe that could easily lead to a short-circuit flow.

The results showed that when the overflow pipe diameter is smaller, in addition to creating difficulty in generating a short-circuit flow, it is also harder for particles to flow out from the overflow exit, thus, obtaining a better supernatant liquid. The drawback is that the relatively small diameter can only allow the flow of a small amount of supernatant liquid. As a result, if the primary objective of clarification requires a large amount of flow, then, one feasible way is to use a convergent type of overflow pipes. Therefore, this study simulated another overflow pipe with a larger convergent angle of 15-9, i.e., a pipe with an overflow entrance of 9 mm and an overflow exit of 15 mm. The separation efficiency is as shown in Fig. 11. In the figure, a comparison with straight pipes 15-15 having a similar exit diameter of 15 mm shows that the amount of particles flowing towards the underflow can be increased by 0.2, which is significantly greater than the previous case at 0.05.

V. CONCLUSION

This study used simulation and experimental verification to determine that a smaller overflow pipe diameter can obtain much more supernatant liquid at the overflow. However, the smaller the overflow pipe diameter, the smaller the amount of supernatant liquid. The study fur-

ther proposed, through simulation, a convergent type 15-9 overflow pipe that can be used to obtain a relatively large amount of supernatant from the overflow liquid. If the objective is to obtain supernatant liquid or solutions with great recycling value, then the appropriate use of a convergent type of overflow pipe is recommended. The advantage is that even with little change in geometry and no significant addition to cost, a much larger amount of supernatant liquid can be obtained.

NOTATION

m_a	mass of arm
$\bar{\phi}$	filtered variable
D	fluid domain
G	filter function that determines the scale of the resolved eddies
ρ	fluid density
\bar{u}_i	fluid velocity
σ_{ij}	stress tensor
μ	fluid viscosity
τ_{ij}	stress

REFERENCES

1. Delgadillo, J. A. and Rajamani, R. K., "A Comparative Study of Three Turbulence-Closure Models for the Hydrocyclone Problem," *International Journal of Mineral Processing*, Vol. 77, No. 4, pp. 217-230 (2005).
2. Delgadillo, J. A. and Rajamani, R. K., "Hydrocyclone Modeling: Large Eddy Simulation CFD Approach," *Minerals & Metallurgical Processing*, Vol. 22, No. 4, pp. 225-232 (2005).
3. Neesse, Th., Schneider, M., Golyk, V., and Tiefel, H., "Measuring the Operating State of the Hydrocyclone," *Minerals Engineering*, Vol. 17, No. 5, pp. 697-703 (2004).
4. Franks, G. V., Yates, P. D., Lambert, N. W. A., and Jameson, G. J., "Aggregate Size and Density After Shearing, Implications for Dewatering Fine Tailings with Hydrocyclones," *International Journal of Mineral Processing*, Vol. 77, No. 1, pp. 46-52 (2005).
5. Bai, Z. S., Wang, H. L., and Tu, S. T., "Experimental Study of Flow Patterns in Deoiling Hydrocyclone," *Minerals Engineering*, Vol. 22, No. 4, pp. 319-323 (2009).
6. Woodfield, D. and Bickert, G., "Separation of Flocs in Hydrocyclones—Significance of Floc Breakage and

- Floc Hydrodynamics,” *International Journal of Mineral Processing*, Vol. 73, No. 2-4, pp. 239-249 (2004).
7. Honaker, R. Q., Ozsever, A. V., Singh, N., and Parekh, B. K., “Apex Water Injection for Improved Hydrocyclone Classification Efficiency,” *Minerals Engineering*, Vol. 14, No. 11, pp. 1445-1457 (2001).
 8. Changirwa, R., Rockwell, M. C., Frimpong, S., and Szymanski, J., “Hybrid Simulation for Oil-Solids-Water Separation in Oil Sands Production,” *Minerals Engineering*, Vol. 12, No. 12, pp. 1459-1468 (1999).
 9. Lee, M. S. and Williams, R. A., “Performance Characteristics within a Modified Hydrocyclone,” *Minerals Engineering*, Vol. 6, No. 7, pp. 743-751 (1993).
 10. Asomah, A. K. and Napier-Munn, T. J., “An Empirical Model of Hydrocyclones, Incorporating Angle of Cyclone Inclination,” *Minerals Engineering*, Vol. 10, No. 3, pp. 339-347 (1997).
 11. Grommers, H. E., Krikken, J., Bos, B. H., and van der Krogt, D. A., “Comparison of Small Hydrocyclones Based on Total Process Costs,” *Minerals Engineering*, Vol. 17, No. 5, pp. 581-589 (2004).
 12. Shah, H., Majumder, A. K., and Barnwal, J. P., “Development of Water Split Model for a 76 mm Hydrocyclone,” *Minerals Engineering*, Vol. 19, No. 1, pp. 102-104 (2006).
 13. Mainza, A., Powell, M. S., and Knopjes, B., “Differential Classification of Dense Material in a Three-Product Cyclone,” *Minerals Engineering*, Vol. 17, No. 5, pp. 573-579 (2004).
 14. Wang, B. and Yu, A. B., “Numerical Study of the Gas-Liquid-Solid Flow in Hydrocyclones with Different Configuration of Vortex Finder,” *Chemical Engineering Journal*, Vol. 135, No. 1-2, pp. 33-42 (2008).
 15. Xu, P., Wu, Z., Mujumdar, A. S., and Yu, B., “Innovative Hydrocyclone Inlet Designs to Reduce Erosion-Induced Wear in Mineral Dewatering Processes,” *Drying Technology*, Vol. 27, No. 2, pp. 201-211 (2009).
 16. Yang, W. J., Wang, C. C., Hsu, R. Y., and Wu, R. M., “Two-Phase Flow Simulation of Reactor Clarifiers,” *Journal of the Chinese Institute of Chemical Engineers*, Vol. 39, No. 3, pp. 275-280 (2008).
 17. Slack, M. D., Del Porte, S., and Engelman, M. S., “Designing Automated Computational Fluid Dynamics Modeling Tools for Hydrocyclone Design,” *Minerals Engineering*, Vol. 17, No. 5, pp. 705-711 (2004).
 18. Hashmi, K. A., Hamza, H. A., and Wilson, J. C., “CANMET Hydrocyclone: an Emerging Alternative for the Treatment of Oily Waste Streams,” *Minerals Engineering*, Vol. 17, No. 5, pp. 643-649 (2004).

Manuscript Received: Nov. 07, 2012

First Revision Received: Nov. 19, 2012

Second Revision Received: Mar. 04, 2013

and Accepted: Mar. 07, 2013